PCCP

Accepted Manuscript




ROYAL SOCIETY OF CHEMISTRY

www.rsc.org/pccp

PCCP

RSCPublishing

ARTICLE

# Controllable optical transitions of amorphous Mg and Mg-Ni films via electrochemical method

Cite this: DOI: 10.1039/x0xx00000x

Jiameng Qiu,[a] Feilong Wu,[a] Xin Jin,[a] Xinyuan Gu,[a] WenBin Cai,[b] Dalin Sun,[a] Fang Fang*[a]

Received ooth January 2012,
Accepted ooth January 2012

DOI: 10.1039/x0xx00000x

www.rsc.org/

Amorphous Mg and $MgNi_x$ ($0.03 \leqslant x \leqslant 0.30$) thin films capped with Pd were prepared by magnetron co-sputtering and their hydrogen-induced optical transition were investigated via electrochemical charging and discharging in KOH electrolyte. The repetitive transitions up to dozens of times between mirror state and transparent state are achieved in amorphous Mg and $MgNi_x$ thin films even though some performance degenerations obtain during cycling. These deteriorations are mainly attributed to the breakdown of film structure caused by both a large change in film volume during cycling and the corrosive attack of KOH electrolyte. In addition, the calculation based on electrochemical stripping method indicates that the hydrogen diffusion coefficient is significantly increased by amorphization while only slightly improved by adding Ni. Among these prepared amorphous films, the $MgNi_{0.09}$ film shows a largest hydrogen diffusion coefficient, namely $2.64\times10^{-13}$ $cm^2/s$. More importantly, the optical properties of amorphous Mg and $MgNi_x$ films are readily manipulated in the charging process, especially under a small charging current density where there is a linear correlation between charging capacity and transmittance. This tunable optical properties obtained in the present work will greatly expand the application fields of Mg-based thin films.

## Introduction

The reversible switching between a mirror, low-impedance state and a transparent, high-impedance one by controlling hydrogen concentration in a thin film is called "switchable mirror" effect. In 1996, Huiberts et al. first discovered this "switchable mirror" effect in palladium capped yttrium thin film between trihydride and dihydride states.[1] Following this observation, similar optical and electrical transitions have also been achieved on Gd,[2] Y-Mg,[3,4] La-Co,[5] Gd-Mg,[6,7] Mg-Ni,[8,9] Mg-Ti,[10,11] Mg-Co[12,13] thin films and so on upon hydrogen loading and unloading. These materials with "switchable mirror" effect provide potential applications in fabricating new photoelectric devices, such as hydrogen sensor, solar collection and 'smart' window.[14,15]

So far, three generations of hydrogen-induced switchable thin film, i.e., rare earth thin films,[1,2] rare earth alloy thin films[3–7] and Mg-based alloy thin films,[8–13] had been developed and their optical and electrical transitions properties were investigated. For instance, Isidorsson et. al. reported that by exposing to hydrogen gas, the transmittance and resistivity of LaMg film can be changed from 2% and 0.6 mΩ·cm to about 40% and 1.2 mΩ·cm, respectively.[16] Kumar el. al. showed that $Mm_{0.2}Tb_{0.8}Co_2$ alloy thin film switched from the mirror state to a transparent state via electrochemical hydrogenation in KOH electrolyte with a switching time of 50 s.[5] Moreover, all-solid-state switchable mirrors based on Mg-Ti or Mg-Ni thin films were prepared by Tajima el. al. and showed thousands of reversible transition by applying positive or negative voltage.[14,15] These thin films with "switchable mirror" effect can be reversibly switched between mirror state and transparent state via alternately introducing hydrogen gas and air or electrochemical method. However, the relationship between hydrogen concentration and optical properties is still ambiguous owing to the following two reasons: i) during gas-phase loading and unloading, it is difficult to measure accurately and control the amount of absorbed hydrogen because of the very small mass changes associated with thin films; ii) although electrochemical hydrogenation in both liquid and solid electrolyte can control the hydrogen concentration accurately on the basis of the charge transfer, most of studies using electrochemical method focus on switching response and cycle stability and pay little attention to the relationship between hydrogen concentration and optical properties. As a result, optical properties are not controllable except for the full hydrogenation and full dehydrogenation states. This uncontrollability of optical properties greatly limits the applications of hydrogen-induced switchable thin films, especially makes against the 'smart' window that requires continuously variable transmittance with high controllability.[17–20] Therefore, realization in the controllability of optical properties by hydrogen concentration are urgently needed from a fundamental perspective as well as for potential application.

Moreover, recently, our group found that amorphization and Ni addition can efficiently enhance the hydrogen loading/unloading kinetics of Mg and Mg–Ni thin films and the switching response of thin films was observed to first decrease, pass through a minimum and then increase with increasing Ni content.[21] For instance, among amorphous $MgNi_x$ (x = 0.03–0.3) films, the fastest switching response from mirror state to transparent state was 26 s for the amorphous $MgNi_{0.09}$ film, which was about one tenth of 216 s for crystalline $MgNi_{0.09}$ film under the same hydrogenation conditions.

This obtained kinetics improvement was suggested to be mainly related to the catalysis of Ni and the faster hydrogen diffusion caused by amorphization. Nevertheless, no direct experimental evidence was obtained during gas-phase loading and unloading to support this suggestion and the contribution of Ni addition to the improvement of hydrogen diffusion was unclear. Previous researches on crystalline Mg and Mg-Ti thin films for hydrogen storage have shown that the hydrogen diffusion coefficient can be measured conventionally by electrochemical measurement.[22,23] Hence, studies of the hydrogen diffusion inside amorphous Mg and Mg–Ni thin films via electrochemical method have been performed to distinguish the different effects of amorphization and Ni addition.

In the study, we investigate the optical transition of amorphous Mg and Mg–Ni thin films by electrochemical method. It reveals that the hydrogen diffusion is accelerated considerably by amorphization and slightly by Ni addition and the transparent state can be modulated by controlling the hydrogen concentration, i.e., charging capacity during charging process under a small current density.

## Experimental section

### Films Preparation

Mg and Mg–Ni films were deposited onto Si or ITO substrates without heating process in a 4-gun DC/RF magnetron co-sputtering system, and *in situ* capped with a 15- nm thick Pd layer to protect the films from oxidation and catalyze de-/hydrogenation. The thickness of Mg or Mg–Ni films was set to be about 200 nm and was confirmed by step profiler after deposition. Mg film and four $MgNi_x$ ($0 < x \leq 0.30$) films were prepared by adjusting the sputtering power of Ni. Typical deposition rates were 9.5 Å/s for Mg (200 W RF power), 0–2.7 Å/s for Ni (0–42 W DC power), and 2 Å/s for Pd (180 W RF power). Additional inductively coupled plasma mass spectroscopy showed that the atomic ratios (x) of Mg to Ni in $MgNi_x$ films were 1:0.03, 1:0.09, 1:0.21, and 1:0.30, respectively. In addition, during the deposition of $MgNi_{0.09}$ film, quartz crystals with a mask were placed next to the substrates to ex-situ measure the weight of deposited film based on the quartz-crystal microbalance method which had been described elsewhere.[21,24] The area of $MgNi_{0.09}$ film on quartz crystals was set to be $0.3\times0.3\times\pi$ $cm^2$ by the mask and the average weight is calculated to be 55 μg based on the frequency shift, suggesting that the density of prepared $MgNi_{0.09}$ films with a thickness of 200 nm was 0.973 $g/cm^3$.

### Structural characterization and properties measurements

The electrochemical experiments were performed on a CHI 660 electrochemical workstation in 6 M or 1 M KOH electrolyte in a three-electrode cell at 298 K. The working, counter and reference electrodes were Mg-Ni films, $Ni(OH)_2$/NiOOH foil and saturated Hg/HgO electrode, respectively. Before electrochemical experiment, the KOH electrolyte was purged with high purity argon for 30 min to eliminate the influence of oxygen. During electrochemical experiments, the transmittance of Mg and $MgNi_x$ films was *in-situ* monitored by a combined use of a laser diode ($\lambda$ = 535 nm) and a Si photodiode. After electrochemical experiments, thin films were washed by deionized water and blow-dried by a nitrogen gas gun in a simple nitrogen-filled glovebox in which the oxygen content is maintained below 100 ppm. The phase structure of Mg and $MgNi_x$ films were characterized by X-ray diffraction (XRD) on a Rigaku D/max 2400 with Cu $K_\alpha$ radiation at 40 kV and 100 mA. An *in-situ* cell was used to isolate oxygen during XRD measurement. The surface features were examined by scanning electron microscopy (SEM, XL30FEG, Philips). The transmission spectra within the wavelength of 200-900 nm were *ex-situ* measured from the top side of the film at room temperature on a Spectroscopy UV-2450 (Shimadzu, Japan). For the electrochemical stripping experiments, Mg and $MgNi_x$ films firstly held at a charge potential of -1.1 V in 1 M KOH for 1 h and subsequently switched to a discharge potential of 0.3 V for another 1 h to measure the anodic current over time.

## Results and discussion

### Structural characterization of Mg and $MgNi_x$ films

The phase structure and surface features of Mg and $MgNi_x$ films before and after electrochemical charging and discharging were examined by XRD and SEM, and the typical results for the $MgNi_{0.09}$ film are shown in Fig. 1. As can be seen in Fig. 1a, no peaks belong to Mg-containing crystalline phases are obtained except for one weak Pd peak in the XRD pattern, suggestive of the amorphous structure of the as-prepared Mg and $MgNi_x$ films. The corresponding SEM image demonstrates that the as-prepared $MgNi_{0.09}$ film has a smooth surface, thus giving a clear mirror image with high reflection as shown in inserted photo (see Fig. 1b). After electrochemical charging, the $MgNi_{0.09}$ film is switched to transparent state without the appearance of hydrides phase as indicated by the XRD pattern in Fig. 1a. Furthermore, the $MgNi_{0.09}$ film returns to mirror state after discharging, whose XRD pattern is the same as that for the as-prepared one, suggesting that amorphous structure can be maintained during electrochemical charging and discharging.

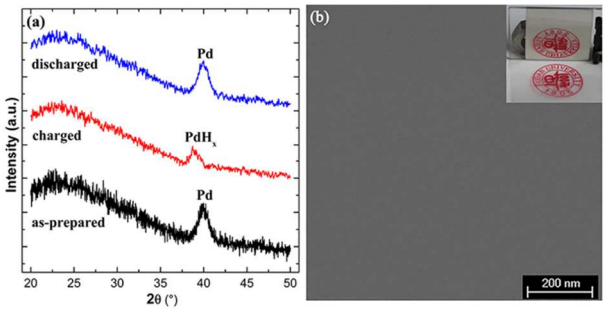


**Fig. 1** (a) XRD patterns for the as-prepared, charged and discharged $MgNi_{0.09}$ film; (b) SEM image and photo for the as-prepared $MgNi_{0.09}$ film.

### Influence of amorphization and Ni addition on hydrogen diffusion coefficient

In order to quantitatively evaluate the hydrogen diffusion inside amorphous films, the hydrogen diffusion coefficients are calculated by the electrochemical stripping method in 1 M KOH solution using Hagi's model.[25,26] For this model, if the discharging time $t$ is long enough ($t > 3L^2/\pi^2 D_H$), the relationship between the anodic current $I$ and hydrogen diffusion coefficient $D_H$ can be described as:

$\ln(I) = -\pi^2 D_H/4L^2 t$+constant

where $L$ is the film thickness. Fig. 2 shows the resulting current responses expressed in $\ln(I)$ vs. $t$ for amorphous Mg and $MgNi_x$ thin films. From Fig. 2a, it can be calculated that the hydrogen diffusion coefficient in the amorphous Mg film is $1.54\times10^{-13}$ $cm^2/s$, about 23 times larger than $6.5\times10^{-15}$ $cm^2/s$ for crystalline Mg film reported by Qu et al.[23] or almost three orders of magnitude larger than $1.1\times10^{-16}$ $cm^2/s$ reported by Spatz et al.[27] Furthermore, after adding a small amount of Ni, the hydrogen diffusion coefficient further increases to $2.23\times10^{-13}$, $2.64\times10^{-13}$, $2.57\times10^{-13}$ and $2.01\times10^{-13}$ $cm^2/s$ for the $MgNi_{0.03}$, $MgNi_{0.09}$, $MgNi_{0.21}$ and $MgNi_{0.30}$ films, respectively. Among various Mg and $MgNi_x$ thin films, the $MgNi_{0.09}$ film yields the largest hydrogen diffusion coefficient, which is consistent with

the fastest optical and electrical response of the $MgNi_{0.09}$ film during hydrogen gas loading.[21] Since the increase of the hydrogen diffusion coefficient by Ni addition in $MgNi_x$ thin films is not more than 71% as compared with amorphous Mg film, it is reasonable to deduce that the hydrogen diffusion is accelerated by both amorphization and Ni addition, but amorphization is more effective than Ni addition.

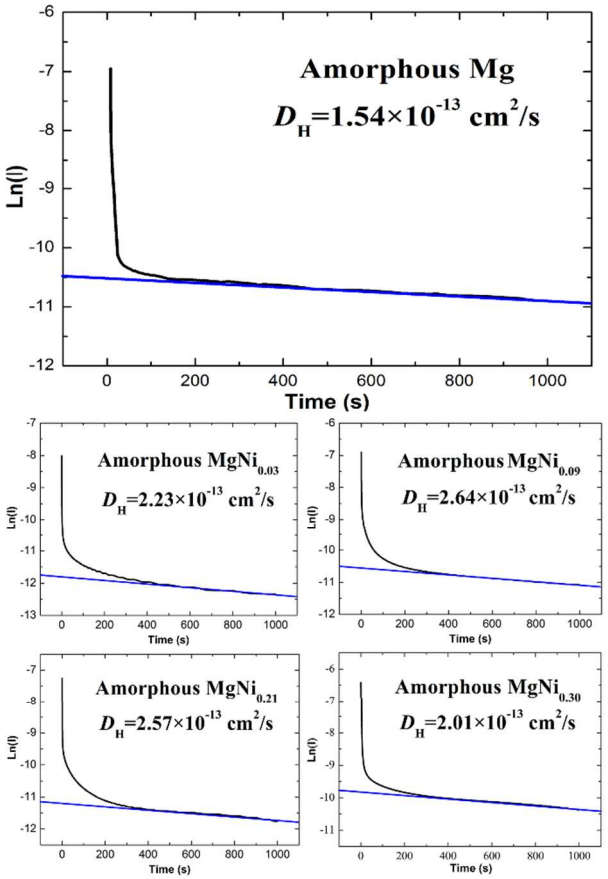


**Fig. 2** Hydrogen stripping curves for amorphous (a) Mg, (b) $MgNi_{0.03}$, (c) $MgNi_{0.09}$, (d) $MgNi_{0.21}$, (e) $MgNi_{0.30}$ thin films.

Moreover, from the transmission spectra for hydrogenated Mg and $MgNi_x$ thin films as shown in Fig. 3, two features can be found: i) as compared with hydrogenated Mg film, the absorption edge for $MgNi_{0.03}$ film remained unchanged and mainly originated from the absorption of quartz substrates, suggesting that Ni in $MgNi_{0.03}$ film mainly acted as catalyst to enhance hydrogen diffusion; ii) when Ni content increased to 0.09, an obvious red shift of the absorption edge was observed. With increasing Ni content from 0.09 to 0.30, the absorption edge further shifted towards longer wavelengths. Considering that the hydrides of Mg-Ni alloy phases have much smaller optical band gaps than $MgH_2$, for instance the optical band gap of 1.75 eV for $Mg_2NiH_4$ is 69% smaller than that of 5.6 eV for MgH,[28,29] the evolution of the absorption edge suggests that except for the Ni as catalyst, part of Ni in $MgNi_{0.09}$, $MgNi_{0.21}$ and $MgNi_{0.30}$ films combines with Mg to form amorphous Mg-Ni alloy phases and the content of the alloy phases becomes increasingly more with the increase of Ni content. However, since the hydrogen diffusion coefficients for Mg-Ni alloy phases are smaller than that for Mg phase,[30] the formation of amorphous Mg-Ni alloy phases would reduce the hydrogen diffusion coefficient. Therefore, the hydrogen diffusion will, on the one hand, be improved by the catalysis of Ni and, on the other hand, be blocked owing to the formation of amorphous Mg-Ni alloy phase. The competition of these two conflicting effects results in that the hydrogen diffusion coefficient first increases and then decreases with increasing Ni content and shows a maximum value of 2.64×10$^{-13}$ cm$^2$/s for the $MgNi_{0.09}$ film. Furthermore, the $MgNi_{0.09}$ film is chosen as a typical sample to investigate the influence of current density on the controllable optical property in the following sections.

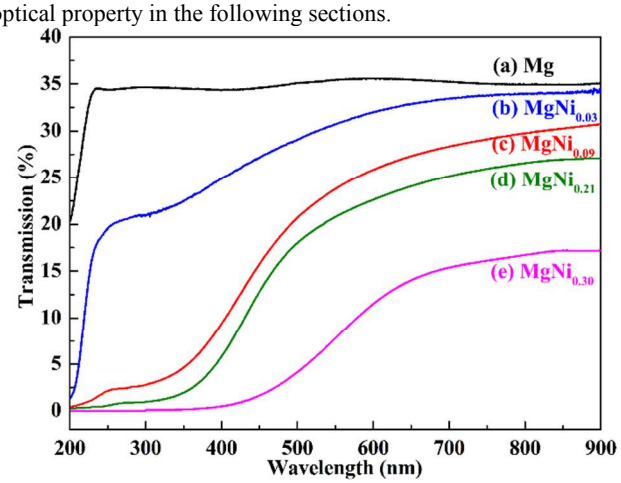


**Fig. 3** Transmission spectra for amorphous (a) Mg, (b) $MgNi_{0.03}$, (c) $MgNi_{0.09}$, (d) $MgNi_{0.21}$, (e) $MgNi_{0.30}$ thin films after hydrogen loading.

### Controllable optical properties

Fig. 4 shows the evolution of transmittance during one cycle of charging and discharging under a small current density of 0.1 mA/cm$^2$. The inserted images in Fig. 4 are the badge of the 'Fudan University'. The left half of the badge is covered by the film and the other half is left blank for comparison. Here, it should be noted for these images that underexposure was used to clearly show the badge at the transparent state and thus the film looked like black more than its real silver at mirror state. In the charging process, it can be seen that the $MgNi_{0.09}$ film gradually changes from mirror state to transparent state as shown in the inserted images and reaches the maximum transmittance of 24.89% after seven charging steps. Interestingly, the increase of transmittance during each charging step is almost same. For instance, the transmittance increases from 0 to 3.9% by 3.9% for the first charging step and from 14.7% to 18.4% by 3.7% for the fifth charging step. This suggests that there is a linear correlation between transmittance and charging capacity (i.e., hydrogen content based on charge transfer). It is noted that this linear correlation is quite different with the exponential growth of the transmittance in the previous reports for crystalline Mg-Ni films by gas-phase hydrogenation.[9,31] This difference can be understood from two factors: i) the prepared amorphous $MgNi_{0.09}$ film has much faster hydrogenation kinetics as compared to a crystalline Mg-Ni film with the same thickness; ii) the small charge current density and the interval between two charging steps indicate that the absorbed hydrogen can react with the amorphous $MgNi_{0.09}$ film to produce hydrides before next charging step. Therefore, it can be envisioned that if more hydrogen atoms absorb and diffuse into the film in each charging step, the hydride formation could be dramatically accelerated. In other words, the optical transition of the $MgNi_{0.09}$ film from mirror state to transparent state can be significantly accelerated with an increased charging current density, which will be further investigated in the next section.

In the discharging process as shown in Fig. 4b, it can be observed that the transmittance gradually decreases and the film returns to mirror state. However, differing with linear relationship between the transmittance and charging capacity in charging

process, the curve of transmittance resembles the unifoliate hyperbola in Fig. 4b, indicating that the decomposition rate of hydrides gradually drops along with the discharging process given that the transmittance is determined by the content of hydrides. To be specific, at the beginning period of discharging, the hydrides have a relative large decomposition rate and quickly decompose into hydrogen atoms and metal and thus the transmittance reduces rapidly. However, part of the formed hydrogen atoms do not desorb from the $MgNi_{0.09}$ film rather remain dissolved in the film according to the limited charge transfer in first few discharging steps. With increasing discharging steps, the decomposition rate of hydrides becomes smaller and the dissolved hydrogen desorb from the film, resulting in a gentle reduction of transmittance in the later period of discharging. Similar variation tendency in decomposition rate is also reported for other hydrogen storage alloys, such as $La_2MgNi_9$,[32] $Mg_2Ni$[33] and so on. Thus, a question raises that whether the hydride decomposition could be improved by increasing discharging current density, leading to a fast transition from transparent state back to mirror state.

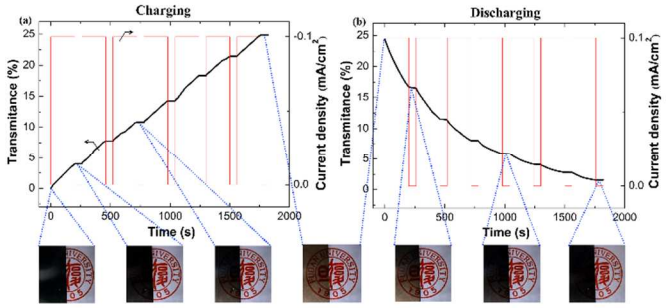


**Fig. 4** The evolution of transmittance of amorphous $MgNi_{0.09}$ film during (a) electrochemical charging and (b) discharging. During the charging and discharging process, a small current density of 0.1 mA/cm$^2$ was applied for 200 s and repeated with an interval of 60 s. The inserted images are the pictures of amorphous $MgNi_{0.09}$ film taken in-situ in KOH electrolyte after several charging or discharging steps.

### Influence of current density on optical properties

To further understand the influence of current density on the hydrides formation and decomposition, the optical transitions of the $MgNi_{0.09}$ film under different charging or discharging current density were investigated and the results are shown in Fig. 5. In the charging process, an apparent plateau is seen from ca. −0.9 V to −1.1 V on the potential curves in Fig. 5a, which corresponds to the hydrogen absorption and hydrides formation. With increasing charging current density from 0.1, 0.2, 0.4, 0.6, 0.8 to 1 mA/cm$^2$, the duration of this potential plateau is shortened from 1500, 740, 337, 145, 86 to 62 s, respectively. The simultaneous monitoring optical signal in Fig. 5b shows that the transmittance gradually climbs across the potential plateau and the response of the $MgNi_{0.09}$ film from mirror state to transparent state is dramatically shorten from 1500, 980, 409, 178, 105 to 79 s when the charging current density increases from 0.1, 0.2, 0.4, 0.6, 0.8 to 1.0 mA/cm$^2$, respectively. Two features can be found from the obvious reduction of response time: i) the hydrides formation is significantly accelerated by increasing charging current density; ii) the transition from mirror state to transparent state is mainly controlled by the charging capacity. In the discharging process, a plateau can be observed at about $E$ = 0.1 V on the potential curve under the discharging current density of 0.1 mA/cm$^2$ in Fig. 5c, which corresponds to the hydrides decomposition and the hydrogen desorption. However, the plateau region is shortened with increasing current density from 0.1 to 0.2 mA/cm$^2$ and disappears when the current density is raised to more than 0.4 mA/cm$^2$. The potential quickly increases to 0.8 to 1.1 V, suggesting the concurrence of unknown side reactions during discharging, such as the oxidation of Pd. From Fig. 5d, it can be observed that the transmittance curves are quite similar under different current density and the response from transparent state back to mirror state is only accelerated from 1200 s to 760 s with increasing current density from 0.1 to 1 mA/cm$^2$, which indicates that discharging current density has little effect on the hydrides decomposition and the transition from transparent state to mirror state is controlled not only by discharging capacity but also by hydrides decomposition. Therefore, considering that the hydride decomposition rate varies with discharging time, we may suggest that the control of the optical property is more feasible in the charging process than in the discharging process, especially under a small charging current density.

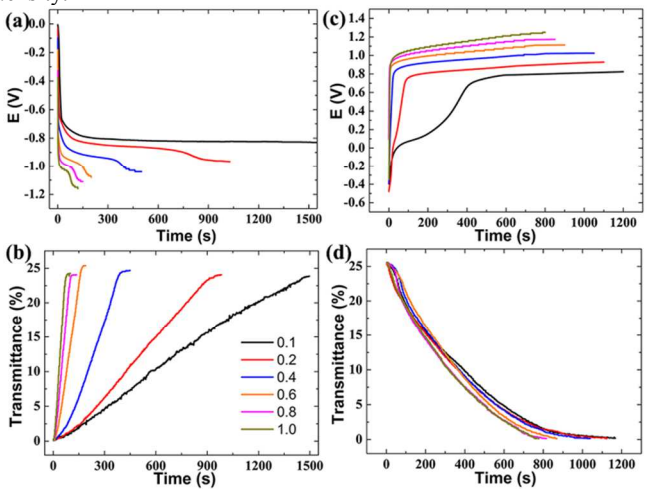


**Fig. 5** Electrode potential and transmittance with time for amorphous $MgNi_{0.09}$ film under 0.1–1.0 mA/cm$^2$ current densities. (a) and (b) for charging process and (c) and (d) for discharging one.

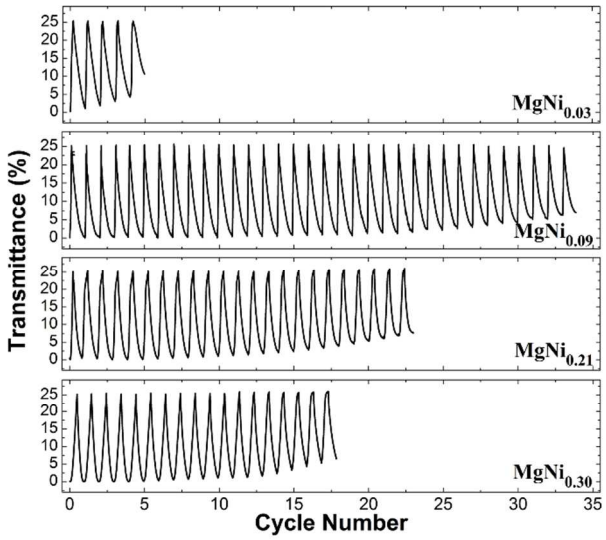


**Fig. 6** The charging and discharging cycles for $MgNi_x$ films.

### Cycling stability of $MgNi_x$ films

The cycling stability of $MgNi_x$ films with repetitive charging and discharging was evaluated and the results are shown in Fig. 6. During the cycling measurement, the current density was set to be 1 mA/cm$^2$ and the charging and discharging times were determined

from the first cycle for each sample. Taking the $MgNi_{0.09}$ film as an example, the charging and discharging time in each cycle are 80 s and 760 s, respectively. During first few cycles, the optical transition of the $MgNi_{0.09}$ film is entirely reversible. With increasing cycle number, the reversibility of optical transition gradually decreases and the transmittance of the $MgNi_{0.09}$ film at its mirror state increases to 6% after 32 cycles (about 25% of the maximum transmittance), suggesting the occurrence of some irreversible reactions and/or the destroy of the film structure. Similar cycling performance can be found for other $MgNi_x$ films, but the valid cycle number reduces to 5, 22 and 18 for the $MgNi_{0.03}$, $MgNi_{0.21}$ and $MgNi_{0.30}$ films, respectively. To understand the invalidation mechanism, the surface features of $MgNi_{0.09}$ and $MgNi_{0.30}$ films after 1, 5 and 15 cycles were characterized by SEM and compared in Fig. 7. From the Fig. 7a and b, it can be found that after 1 cycle, the surface appearance for both the $MgNi_{0.09}$ and $MgNi_{0.30}$ films are still smooth and similar to that for the as-prepared $MgNi_{0.09}$ film shown in Fig. 1b. However, after 5 cycles, the $MgNi_{0.09}$ film in Fig. 7c appears to be roughened but still contiguous while some tiny cracks show up on the surface for the $MgNi_{0.30}$ film(see Fig. 7d). More obvious difference can be found after 15 cycles between Fig. 7e and f, from which some cracks are present on the surface of the $MgNi_{0.09}$ film while many criss-crossing cracks appear on the surface of the $MgNi_{0.30}$ film. This strongly indicates that the breakdown of $MgNi_x$ films is the main reason for the invalidation of optical transition during charging and discharging cycles, which may originate from both the corrosive attack of KOH electrolyte[34] and the large volume change between hydrides and metallic phases.[35]

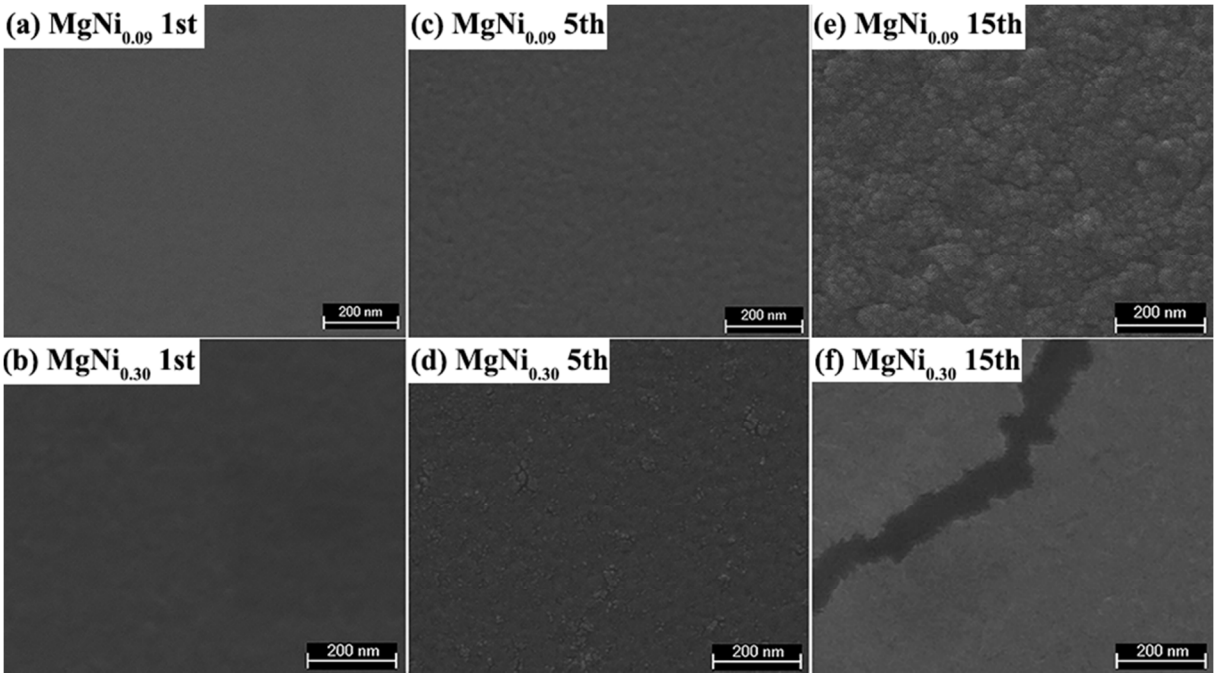


**Fig. 7** SEM images for $MgNi_{0.09}$ and $MgNi_{0.30}$ films after 1, 5 and 15 cycles.

## Conclusions

In this study, we have prepared amorphous Mg and $MgNi_x$ ($0.03 \leq x \leq 0.30$) thin films by magnetron co-sputtering and realized their optical transition between mirror state and transparent state using electrochemical charging and discharging. Three features are observed for amorphous Mg and $MgNi_x$ thin films: i) amorphous Mg and $MgNi_x$ thin films can be reversibly switched from mirror state to transparent state for dozens of times. However, the transmittance at mirror state gradually climbs with increasing cycle number, which is attributed to the breakdown of film structure caused by both the large volume change and the corrosive attack of KOH electrolyte during cycling; ii) the hydrogen diffusion rate is greatly accelerated by amorphization and slightly improved by Ni addition. Among the prepared Mg and $MgNi_x$ films, the largest hydrogen diffusion coefficient of $2.64\times10^{-13}$ $cm^2/s$ is observed for the $MgNi_{0.09}$ film; iii) during the charging process, the transmittance is mainly controlled by charging capacity, especially under a small current density where there is a linear correlation between charging capacity and transmittance. During the discharging process, however, the transition from transparent state back to mirror state is determined not only by discharging capacity but also by hydride decomposition, demonstrating more complexity for controlling the optical properties during discharging. Therefore, it is better to modulate the optical properties in charging process rather than in discharging process. This controllability of the optical properties of amorphous Mg and $MgNi_x$ thin films via electrochemical method is believed to be generally applicable to other switchable mirror thin films and will broaden their scope of potential applications.

## Acknowledgements

This work was financially supported by the National Natural Science Foundation of China (No. 51471052, U1201241), the Science and Technology Commission of Shanghai Municipality (No. 11XD1400600), Guangxi Collaborative Innovation Center of Structure and Property for New Energy Materials and Key Laboratory of Advanced Energy Storage Materials of Guangdong Province.

## Notes and references

[a]Department of Materials Science, Fudan University, 220 Handan Road, Shanghai 200433, China. E-mail: f_fang@fudan.edu.cn
[b]Department of Chemistry, Fudan University, 220 Handan Road, Shanghai 200433, China

1 J. N. Huiberts, R. Griessen, J. H. Rector, R. J. Wijngaarden, J. P. Dekker, D. G. de Groot and N. J. Koeman, *Nature*, 1996, **380**, 231–234.
2 I. Aruna, B. R. Mehta, L. K. Malhotra and S. M. Shivaprasad, *Adv. Mater.* 2004, **16**, 169–173.
3 Y. Yamada, M. Miura, K. Tajima, M. Okada, M. Tazawa and K.Yoshimura, *Thin Solid Films*, 2014, **571**, 712–714.
4 Y. Yamada, M. Miura, K. Tajima, M. Okada and K. Yoshimura, *Sol. Energ. Mat. Sol. C.* 2014, **120**, 631–634.
5 M. K. Kumar, N. Rajalakshmi and S. Ramaprabhu, *J. Phys. Chem. C*, 2007, **111**, 8532–8537.
6 P. van der Sluis and V. M. M. Mercier, *Electrochim. Acta*, 2001, **46**, 2167–2171.
7 R. Armitage, M. Rubin, T. Richardson, N. Obrien and Y. Chen, *Appl. Phys. Lett.*, 1999, **75**, 1863–1865.
8 R. Gremaud, C. P. Broedersz, A. Borgschulte, M. J. van Setten, H. Schreuders, M. Slaman, B. Dam and R. Griessen, *Acta Mater.*, 2010, **58**, 658–668.
9 C. W. Hsu, S. L. Lee, F. K. Hsu and J. C. Lin, *Int. J. Hydrogen Energy*, 2011, **36**, 5383–5387.
10 D. M. Borsa, A. Baldi, M. Pasturel, H. Schreuders1, B. Dam, R. Griessen, P. Vermeulen and P. H. L. Notten, *Appl. Phys. Lett.*, 2006, **88**, 241910.
11 D. M. Borsa, R. Gremaud, A. Baldi, H. Schreuders, J. H. Rector, B. Kooi, P. Vermeulen, P. H. L. Notten, B. Dam and R. Griessen, *Phys. Rev. B*, 2007, **75**, 205408.
12 T. J. Richardson, J. L. Slack, B. Farangis and M. D. Rubin, *Appl. Phys. Lett.*, 2002, **80**, 1349–1351.
13 W. Lohstroh, R. J. Westerwaal, A. C. Lokhorst, J. L. M. van Mechelen, B. Dam and R. Griessen, *J. Alloys Compd.*, 2005, **404–406**, 490–493.
14 K. Tajima, Y. Yamada, S. Bao, M. Okada and K. Yoshimura, *Appl. Phys. Lett.*, 2008, **92**, 041912.
15 K. Tajima, M. Shimoike, H. Li, M. Inagaki, H. Izumi, M. Akiyama, Y. Matsushima and H. Ohta, *Appl. Phys. Lett.*, 2013,**102**,161913.
16 J. Isidorsson, I. A. M. E. Giebels, E. S. Kooij, N. J. Koeman, J. H. Rector, A. T. M. van Gogh and R. Griessen, *Electrochim. Acta*, 2001, **46**, 2179–2185.
17 K. Yoshimura, C. Langhammer and B. Dam, *MRS Bull.*, 2013, **38**, 495–503.
18 K. Yoshimura, Y. Yamada, S. Bao, K. Tajima and M. Okada, *Sol. Energ. Mat. Sol. C.*, 2009, **93**, 2138–2142.
19 R. Baetens, B. P. Jelle and A. Gustavsen, *Sol. Energ. Mat. Sol. C.*, 2010, **94**, 87–105.
20 K. Tajima, Y. Yamada, S. Bao, M. Okada and K. Yoshimura, *Appl. Phys. Lett.*, 2007, **91**, 051908.
21 Q. Y. Zhao, Y. T. Li, Y. Song, X. L. Cui, D. L. Sun and F. Fang, *Appl. Phys. Lett.*, 2013, **102**, 161901.
22 G. B. Xin, J. Z. Yang, C. Y. Wang, J. Zheng and X. G. Li, *Dalton Trans.*, 2012, **41**, 6783–6790.
23 J. L. Qu, Y. T. Wang, L. Xie, J. Zheng, Y. Liu and X. G. Li, *J. Power Sources*, 2009, **186**, 515–520.
24 G. Sauerbrey, *Z. Phys.*, 1959, **155**, 206–222.
25 H. Hagi, *Mater. Trans.*, 1990, **31**, 954–958.
26 Y. Li and Y. T. Cheng, *Int. J. Hydrogen Energy*, 1996, **21**, 281–291.
27 P. Spatz, H. A. Aebischer, A. Krozer and L. Z. Schlapbach, *Z. Phys. Chem.*, 1993, **181**, 393–397.
28 R. J. Westerwaal, M. Slaman, C. P. Broedersz, D. M. Borsa, B. Dam, R. Griessen, A. Borgschulte, W. Lohstroh, R. Kooi, G. ten Brink, K. G. Tschersich and H. P. Fleischhauer, *J. Appl. Phys.*, 2006, **100**, 063518.
29 J. Isidorsson, I. A. M. E. Giebels, H. Arwin and R. Griessen, *Phys. Rev. B*, 2003, **68**, 115112.
30 J. Čermák and L. Král, *Acta Mater.*, 2008, **56**, 2677–2686.
31 R. Gremaud, J. L. M. van Mechelen, H. Schreuders, M. Slaman, B. Dam and R. Griessen, *Int. J. Hydrogen Energy*, 2009, **34**, 8951–8957.
32 M. Latroche, F. Cuevas, W. K. Hu, D. Sheptyakov, R. V. Denys and V. A. Yartys, *J. Phys. Chem. C*, 2014, **118**, 12162–12169.
33 F. Hu, Y. H. Zhang, Y. Zhang, Y. Cai, J. Y. Xu and Z. H. Hou, *J, Mater. Res.*, 2013, **28**, 2701–2708.
34 J. L. Xu, D. Niu and Y. J. Fan, *J. Power Sources*, 2012, **198**, 383–388.
35 D. M. Gattiaa, A. Montonea and L. Pasquini, *Int. J. Hydrogen Energy*, 2013, **38**, 1918–1924.



 